ORIGINAL PAPER

Continuous hysteresis model using Duffing-like equation

Jia-Ying Tu · Pei-Yang Lin · Tsu-Yun Cheng

Received: 21 June 2014 / Accepted: 16 January 2015 / Published online: 11 February 2015 © Springer Science+Business Media Dordrecht 2015

Abstract Many material and mechanical systems, such as magnetorheological (MR) dampers used for reducing vibration in engineering systems, have longstanding modeling and control problems because of their nonlinear hysteresis behavior. Existing hysteresis models, including discontinuous and piecewisecontinuous functions, are nonideal for numerical computation, stability analysis, and control design. This study links the hysteresis characteristics of a Duffinglike equation and an input-output system through a very subtle observation. Thus, the hysteresis dynamics are approximated using a traceable, second-order nonlinear ordinary differential equation with an inertial element. In addition, the hysteresis stability associated with energy dissipation can be analyzed using the Lyapunov method in a more deterministic and systematic manner than has previously been possible. Experimental work and hysteresis identification of a realistic MR damper device are presented to illustrate the proposed Duffing-like modeling techniques.

Keywords Duffing equation · Hysteresis · Magnetorheological damper

J.-Y. Tu (☒) · T.-Y. Cheng Department of Power Mechanical Engineering, National Tsing Hua University, Hsinchu City 300, Taiwan, R.O.C. e-mail: jytu@pme.nthu.edu.tw

P.-Y. Lin

National Center for Research on Earthquake Engineering, Taipei 106, Taiwan, R.O.C.

1 Introduction

Various techniques for modeling hysteresis dynamics in the time domain, including Bingham plastic/biplastic [1–3], nonlinear biviscous [2,4], nonlinear viscoelastic-plastic [2,5], Bouc-Wen [1,6–11], LuGrebased [12], ant other dynamics-based models [13,14], have been proposed. Although these models have been successfully used to describe a wide class of hysteresis and magnetorheological (MR) systems, they exhibit problems when used for parameter identification, numerical computation, stability analysis, and design optimization because these nonideal mathematical models combine a class of elementary functions [15] that can be untraceable, nondeterministic, discontinuous, and lack physical meaning, such as tanh, signum, and absolute functions. Although several studies have attempted to improve modeling efficacy and accuracy, an extremely fundamental problem remains in practice; the use of these effective models, which involve discontinuous and piecewise fitting functions, is disadvantageous for deterministically and systematically developing control system by using dynamicsbased and frequency-dependent techniques.

This study involves modifying the Duffing equation to model hysteresis dynamics. The Duffing oscillator is a well-known, continuous, second-order nonlinear ordinary differential equation that was proposed in 1918 [16]. The typical form of the Duffing equation is expressed by [17–19]



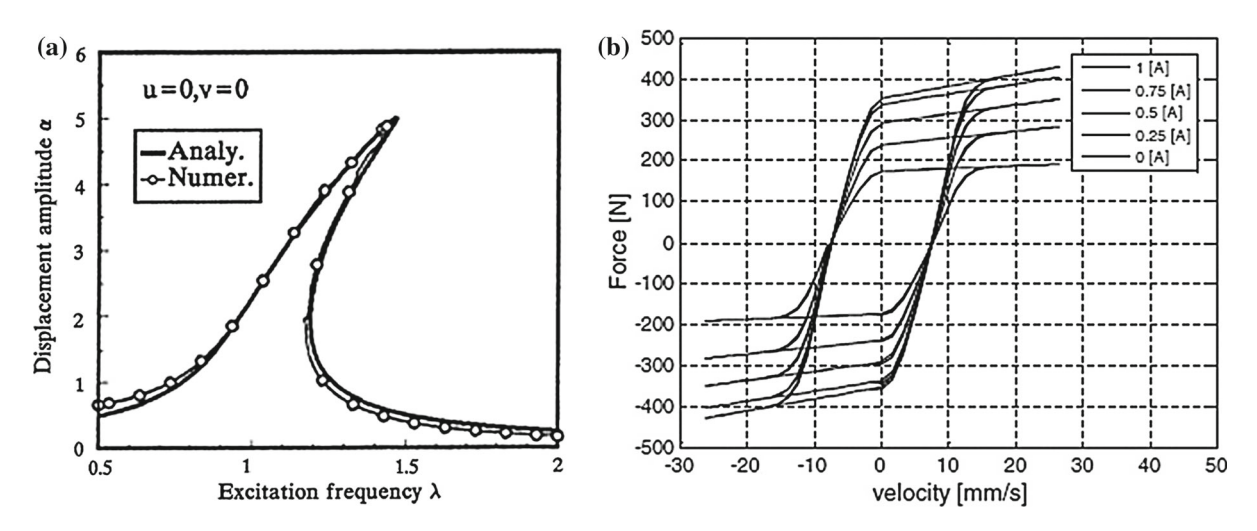


Fig. 1 Analysis of hysteresis dynamics. a Frequency-domain analysis of a Duffing equation [18] and b time-domain analysis of an MR damper [10]

$$\ddot{x} + \gamma \dot{x} + \alpha x + \beta x^3 = F \tag{1}$$

where x denotes the displacement, and \dot{x} and \ddot{x} are the first and second derivatives of x with respect to time. On the right-hand side of Eq. (1), F is the external driving force, and it can be expressed as a harmonic excitation as follows

$$F = A\sin\omega t \tag{2}$$

where A is the magnitude of F, and ω is the excitation frequency. Thus, linear damping and spring forces are controlled by γ and α , respectively. Unlike a simple harmonic oscillator, β in Eq. (1) is an additional coefficient associated with the nonlinear restoring force term x^3 , which considerably influences the system's behavior. When $\beta>0$, the system is considered a hardening spring, and when $\beta<0$, the system is considered a softening spring.

Duffing equation has been used to discuss the behavior of chaotic dynamics, hardening springs, structural systems under magnetic excitation [20], and microelectromechanical systems [21]. Most studies have focused on frequency-dependent techniques, such as that shown in Fig. 1a [18], which shows the typical resonance responses associated with hysteresis effects in the frequency domain. Nevertheless, for the modeling and control applications of many mechanical and material devices, hysteresis identification is conducted in the time domain. For example, Fig. 1b [10] shows

the hysteresis response of an MR damper, where the horizontal and vertical axes indicate the velocity and force data, respectively. Therefore, the comparison of Fig. 1a and b motivated the use of the Duffing equation for hysteresis modeling and analysis in the time domain. Section 2 presents a modification of the Duffing equation. Identification results and parameter fitting of a realistic 3-kN MR damper are discussed in Sect. 3 to validate the proposed techniques. Finally, the conclusion is stated in Sect. 4.

2 Duffing-like equation for modeling hysteresis dynamics

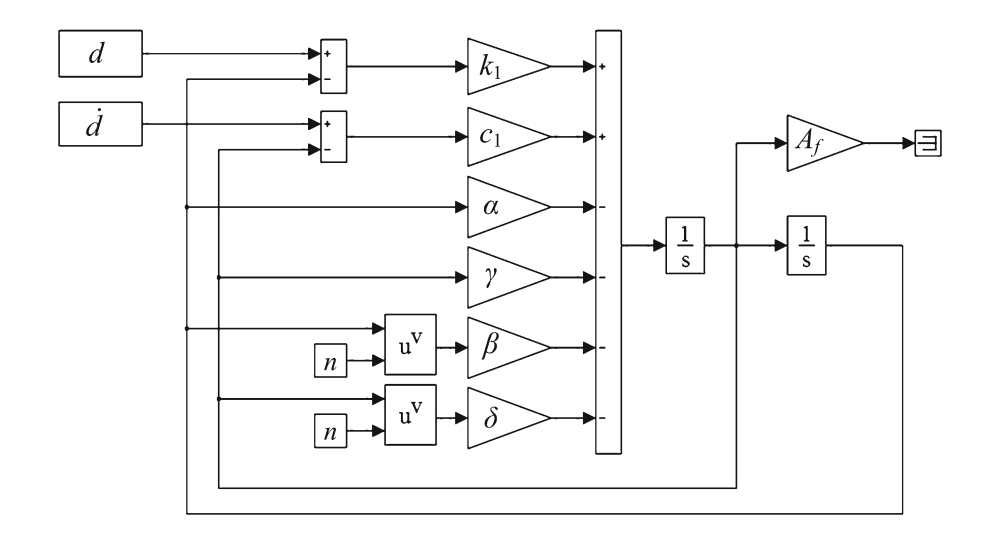
Based on the Duffing equation for time-domain analysis, a deterministic governing equation for hysteresis dynamics is proposed as follows

$$\ddot{x} + \gamma \dot{x} + \alpha x + \beta x^n + \delta \dot{x}^n = k_1 d + c_1 \dot{d}$$
 (3)

where n is the power and should be an odd number. Equation (3) differs from a typical Duffing equation in that a nonlinear element, \dot{x}^n , is added because hysteresis dynamics are rate dependent. For complex cases, n can be different with respect to x and \dot{x} for parameter refinement. Furthermore, the driving force in Eq. (3) is modeled via a dynamics-equivalent spring-damping component, with the parameters k_1 and c_1 ; thus, d and \dot{d} correspond to the input displacement and velocity,



Fig. 2 Simulink model of the Duffing-like equation



respectively. The hysteresis system of Eq. (3) is transformed into an exact input–output dynamic system in state-space form, given by

$$\underbrace{\begin{bmatrix} \dot{x}_1 \\ \dot{x}_2 \end{bmatrix}}_{\dot{\mathbf{x}}} = \underbrace{\begin{bmatrix} 0 & 1 \\ -\alpha & -\gamma \end{bmatrix}}_{\mathbf{A}} \underbrace{\begin{bmatrix} x_1 \\ x_2 \end{bmatrix}}_{\mathbf{x}} + \underbrace{\begin{bmatrix} 0 \\ -\beta x_1^n - \delta x_2^n \end{bmatrix}}_{\mathbf{f}(\mathbf{x})} + \underbrace{\begin{bmatrix} 0 & 0 \\ k_1 & c_1 \end{bmatrix}}_{\mathbf{B}} \underbrace{\begin{bmatrix} \dot{d} \\ \dot{d} \end{bmatrix}}_{\mathbf{d}} \tag{4}$$

$$y = \underbrace{\begin{bmatrix} 0 \ A_f \end{bmatrix}}_{\mathbf{C}} \underbrace{\begin{bmatrix} x_1 \\ x_2 \end{bmatrix}}_{\mathbf{X}} \tag{5}$$

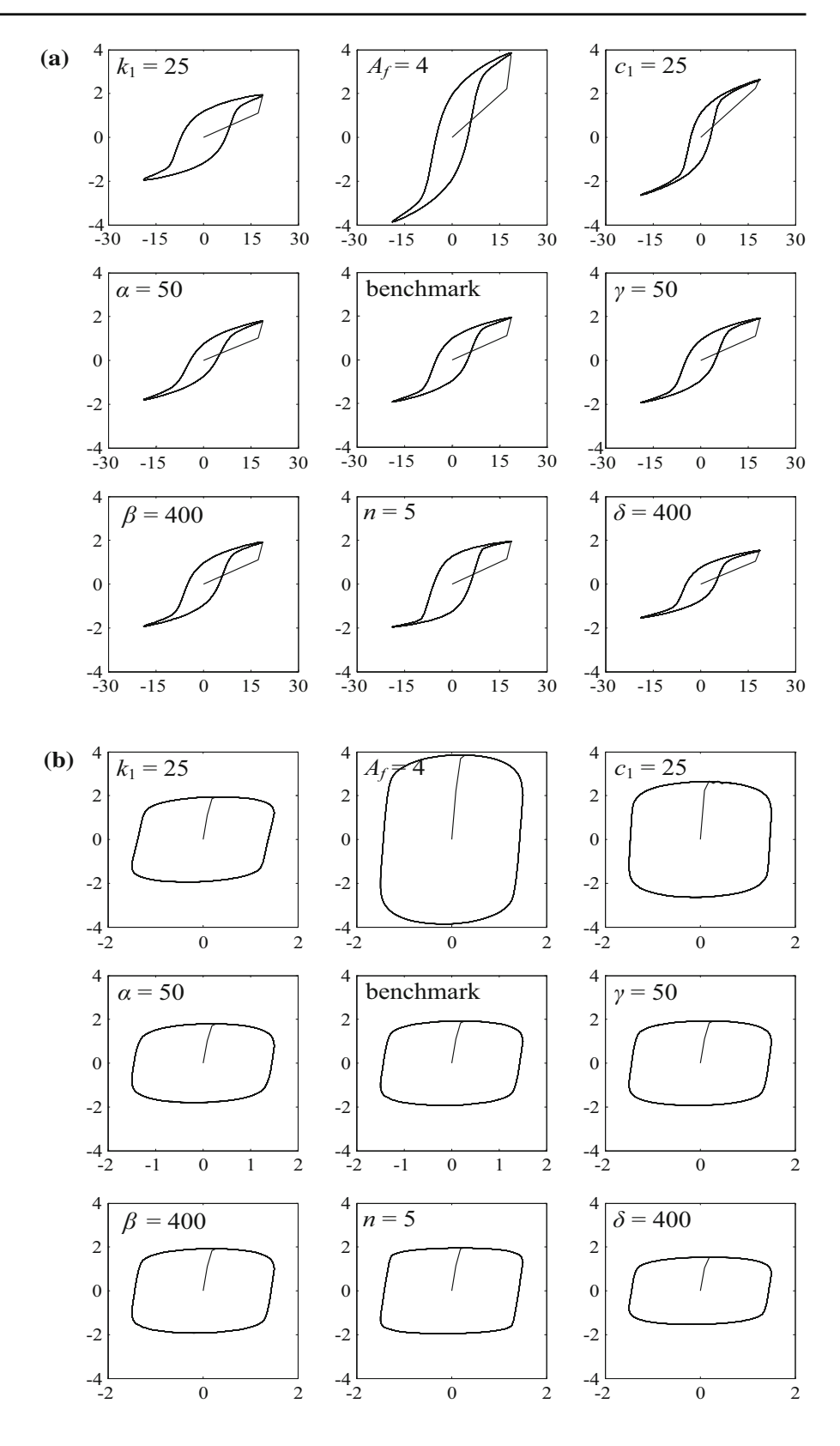
where $x_1 = x$ and $x_2 = \dot{x}$ are state variables and \mathbf{x} is a state vector containing x_1 and x_2 . Accordingly, \mathbf{B} and \mathbf{d} correspond to the input matrix and signal of the hysteresis system, respectively, and \mathbf{C} and y denote the hysteresis output matrix and signal, respectively. The plant and nonlinear dynamics are characterized by \mathbf{A} and $\mathbf{f}(\mathbf{x})$, respectively. According to a subtle observation, the hysteresis output is extracted and linked to the velocity state x_2 through multiplication with a constant A_f ; here, A_f is defined as the maximum amplitude of y. This relation is difficult to detect through the typical analysis of the Duffing equation based on frequency-dependent methods.

According to the expressions in Eqs. (3)–(5), the Simulink model shown in Fig. 2 was used for simulation studies, and the $\dot{d}-y$ and d-y graphs are shown in Fig. 3a and b, respectively. For this comparison, parameters $k_1=c_1=\gamma=\alpha=10, \beta=\delta=$

200, n = 3, and $A_f = 2$ were selected for the benchmark model. To investigate the influence of parameters on the hysteresis curve, each parameter value was increased individually and separately, and the remaining parameters were unchanged. Here, k_1 and c_1 were raised to 25, and γ and α were promoted to 50; in addition, β and δ were doubled, and n = 5 and $A_f = 4$ were assigned. The first column of Fig. 3a indicates that the stiffness-related parameters, k_1 , α , and β , control the width of the hysteresis area. Here, k_1 had a major influence on changing the loop area, whereas a greater α slightly reduced the pre-yield width. In the third column of Fig. 3a, the damping-related parameters, c_1 , γ , and δ , modulated the y-axis magnitude. In particular, an increase in c_1 amplified the y-axis value, whereas the doubling of δ reduced the y-axis magnitude. In the second column, a sharp turning between the post- and pre-yield sections was adjustable according to n, and A_f expanded the y-axis magnitude. On the basis of the observation in Fig. 3, the tuning procedure is described as follows. First, A_f is determined on the basis of the maximum amplitude of y obtained from the measured data, and an odd n is assigned with respect to the turning angle between post- and pre-yield areas. Second, c_1 and k_1 , which control the hysteresis shape, are estimated. Third, γ and δ , which are associated with the rate-dependent dynamics, are chosen. Finally, α and β are considered in a later stage for model refinement. Figure 4a summarizes the tuning procedure for the Duffing-like equation. More detailed study of parameter identification is currently underway.



Fig. 3 Responses of the Duffing-like equation, where the parameters for the benchmark model are $k_1 = c_1 = \gamma = \alpha = 10$, $\beta = \delta = 200$, n = 3, and $A_f = 2$. The other plots surrounding the benchmark model show that the responses varied with parameters. $\mathbf{a} \, \dot{d} - y$ diagrams and $\mathbf{b} \, d - y$ diagrams





(a)
$$\frac{\text{Step 1}}{\text{Step 2}} \frac{A_f \ n}{k_1 \ c_1}$$
 (b) $\frac{\text{Step 1}}{\text{Step 2}} \frac{A_f \ n}{k_1 \ c_1}$ $\frac{\text{Step 2}}{\text{Step 3}} \frac{k_1 \ c_1}{\delta}$ $\frac{c_2}{c_3}$ $\frac{c_2}{\text{Step 4}} \frac{c_3}{\beta}$

Fig. 4 Parameter tuning procedure for the Duffing-like equation. **a** The typical Duffing-like equation. **b** The modified Duffing-like equation for MR damper

The Duffing-like equation provides a more systematic and deterministic foundation for stability analysis than has previously been possible. Here, the widely accepted, direct Lyapunov method is introduced to analyze the hysteresis stability, assuming that γ , δ , α , and β are positive. According to Eq. (4), a typical state-based Lyapunov function for the Duffing-like equation and its first time derivative are given as follows

$$V = \frac{\alpha}{2}x^2 + \frac{1}{2}\dot{x}^2 + \frac{\beta}{n+1}x^{n+1}$$

$$\dot{V} = \dot{x}\ddot{x} + \alpha x\dot{x} + \beta x^n\dot{x}$$

$$= \dot{x}\left(-\alpha x - \gamma \dot{x} - \beta x^n - \delta \dot{x}^n\right) + \alpha x\dot{x} + \beta x^n\dot{x}$$

$$= -\gamma \dot{x}^2 - \delta \dot{x}^{n+1}$$
(7)

Equation (6) is a globally unbounded, positive-definite function, and Eq. (7) shows a negative semi-definite function. In addition, the present study defined a different Lyapunov function on the basis of kinetic and potential energies; this globally unbounded function is written as

$$V = \frac{1}{2}\dot{x}^2 + \int_0^x (\alpha x + \beta x^n) dr$$

= $\frac{1}{2}\dot{x}^2 + \frac{1}{2}\alpha x^2 + \frac{\beta}{n+1}x^{n+1}$ (8)

Thus, the first derivative of Eq. (8) with respect to time yields

$$\dot{V} = \dot{x}\ddot{x} + \alpha x\dot{x} + \beta x^n \dot{x}
= \dot{x} \left(-\alpha x - \gamma \dot{x} - \beta x^n - \delta \dot{x}^n \right) + \alpha x \dot{x} + \beta x^n \dot{x}
= -\gamma \dot{x}^2 - \delta \dot{x}^{n+1}$$
(9)

Equations (6)–(9) show identical V and \dot{V} , and both Eqs. (7) and (9) are negative semi-definite. Thus, the hysteresis system is guaranteed to be asymptotically stable except for the set that \dot{V} is zero. To investigate the stability related to $\dot{V}=0$ and to prove the asymptotical stability of the entire hysteresis system, the invariant set

principle [22] was used. First, the invariant set, denoted as **R**, includes all the solutions that \dot{V} is zero; thus, according to Eqs. (7) and (9), the invariant set is defined as $\dot{x} = 0$, excluding the imaginary solutions. Second, assuming that \dot{x} is zero, Eq. (3) is reduced to

$$\ddot{x} = -\alpha x - \beta x^n \tag{10}$$

In phase plane, the points where \dot{x} and \ddot{x} are zero constitute the domain of attraction. Therefore, Eq. (10) shows that the origin where $\dot{V}=0$ and $x=\dot{x}=\ddot{x}=0$ is the only attractive point and the largest invariant set in **R**. As a result, the hysteresis dynamics are proven to be globally asymptotical stable with continuous energy dissipation, for all positive γ , δ , α , and β .

3 Identification studies of a 3-kN MR damper

To validate and exemplify the proposed techniques in a straightforward and practical manner, a 3-kN MR damper [23] was modeled and its parameters were identified. Controllable MR fluids composed of magnetizable particles and carrying oil (mainly iron particles and silicon oil) are widely used in developing damping devices for vibration reduction. Typically, the MR damper cylinder is filled with an MR fluid, and the piston is wrapped with coils. A voltage-current converter is connected to the coil to generate magnetic fields that align the suspended iron particles. Thus, the effective stiffness of the MR fluid is adjustable in milliseconds by changing the coil current, and the linear, freeflowing MR fluid behaves like a semi-solid. Because the rheological process is reversible and controllable and requires low power, an MR damper combines the advantages of intelligent adaption, such as that of active vibration control, with high reliability, such as that of passive isolators. However, the rheological properties, which depend on many complex factors, related to fluid mechanics, applied electromagnetism, and mechanical design are difficult to model.

In using the Duffing-like equation to model MR damper dynamics, first, a passive case was considered, meaning that the MR fluid was exposed to a constant magnetic field generated by a fixed voltage signal. With reference to Eq. (3), a continuous physical model for an MR damper is proposed in Fig. 5, where the piston shaft is connected to a protected structure, and the bottom of the MR damper is fixed to the ground. Thus,



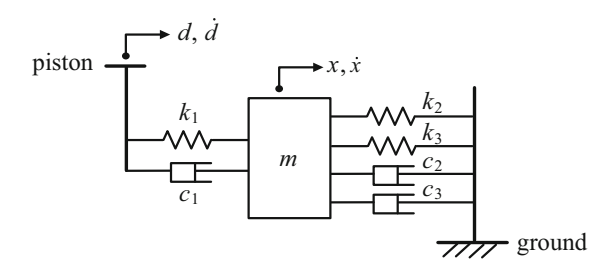


Fig. 5 Proposed MR damper model based on the concept of a Duffing-like equation

the input signals of the piston displacement and velocity are denoted by d and \dot{d} , respectively. In addition, m is assumed to be the total mass of the suspended particles in the MR fluid, and x and \dot{x} are considered the displacement and velocity of the mass, respectively. Parameters k_1 , k_2 , k_3 , c_1 , c_2 , and c_3 represent the associated linear/nonlinear stiffness and damping coefficients. According to Fig. 5 and Eq. (3), the deterministic governing equation for MR damper dynamics is proposed as follows

$$m\ddot{x} + c_2\dot{x} + k_2x + k_3x^n + c_3\dot{x}^n$$

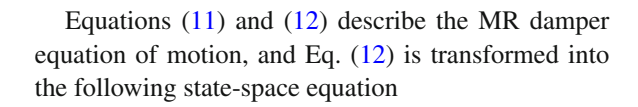
= $k_1(d-x) + c_1(\dot{d}-\dot{x})$ (11)

Furthermore, to conduct parameter identification in a straightforward manner, without considering unit conversion, Eq. (11) is divided by m and normalized to

$$\ddot{x} + \underbrace{(c_1 + c_2)}_{\gamma} \dot{x} + \underbrace{(k_1 + k_2)}_{\alpha} x + \underbrace{k_3}_{\beta} x^n + \underbrace{c_3}_{\delta} \dot{x}^n$$

$$= \underbrace{k_1 d + c_1 \dot{d}}_{F}$$
(12)

Thus, k_1 , k_2 , k_3 , c_1 , c_2 , and c_3 in the rest of this paper are dimensionless constants. The arrangement in Eq. (12) is similar to the Duffing-like system shown in Eq. (3), where the external driving force is expressed on the right-hand side in relation to the applied piston displacement and velocity. In practice, the input velocity signal d can be obtained through differentiation of the d signal. Unlike many existing MR damper models, in Fig. 5 and Eqs. (11) and (12), x is defined as the invisible and immeasurable displacement of the fluid mass, and d is defined as the piston displacement. In addition, the definition of m is different from that in reference [14]; the mass of piston is not considered in the hysteresis dynamics. In this scenario, the MR damper is considered a second-order dynamic equation with kinetic energy attributable to m, rather than a first-order energy dissipation device.



$$\underbrace{\begin{bmatrix} \dot{x}_1 \\ \dot{x}_2 \end{bmatrix}}_{\dot{\mathbf{x}}} = \underbrace{\begin{bmatrix} 0 & 1 \\ -k_1 - k_2 - c_1 - c_2 \end{bmatrix}}_{\mathbf{A}} \underbrace{\begin{bmatrix} x_1 \\ x_2 \end{bmatrix}}_{\mathbf{x}} + \underbrace{\begin{bmatrix} 0 & 0 \\ -c_3 x_2^n - k_3 x_1^n \end{bmatrix}}_{\mathbf{f}(\mathbf{x})} + \underbrace{\begin{bmatrix} 0 & 0 \\ k_1 & c_1 \end{bmatrix}}_{\mathbf{B}} \underbrace{\begin{bmatrix} d \\ \dot{d} \end{bmatrix}}_{\mathbf{d}} \quad (13)$$

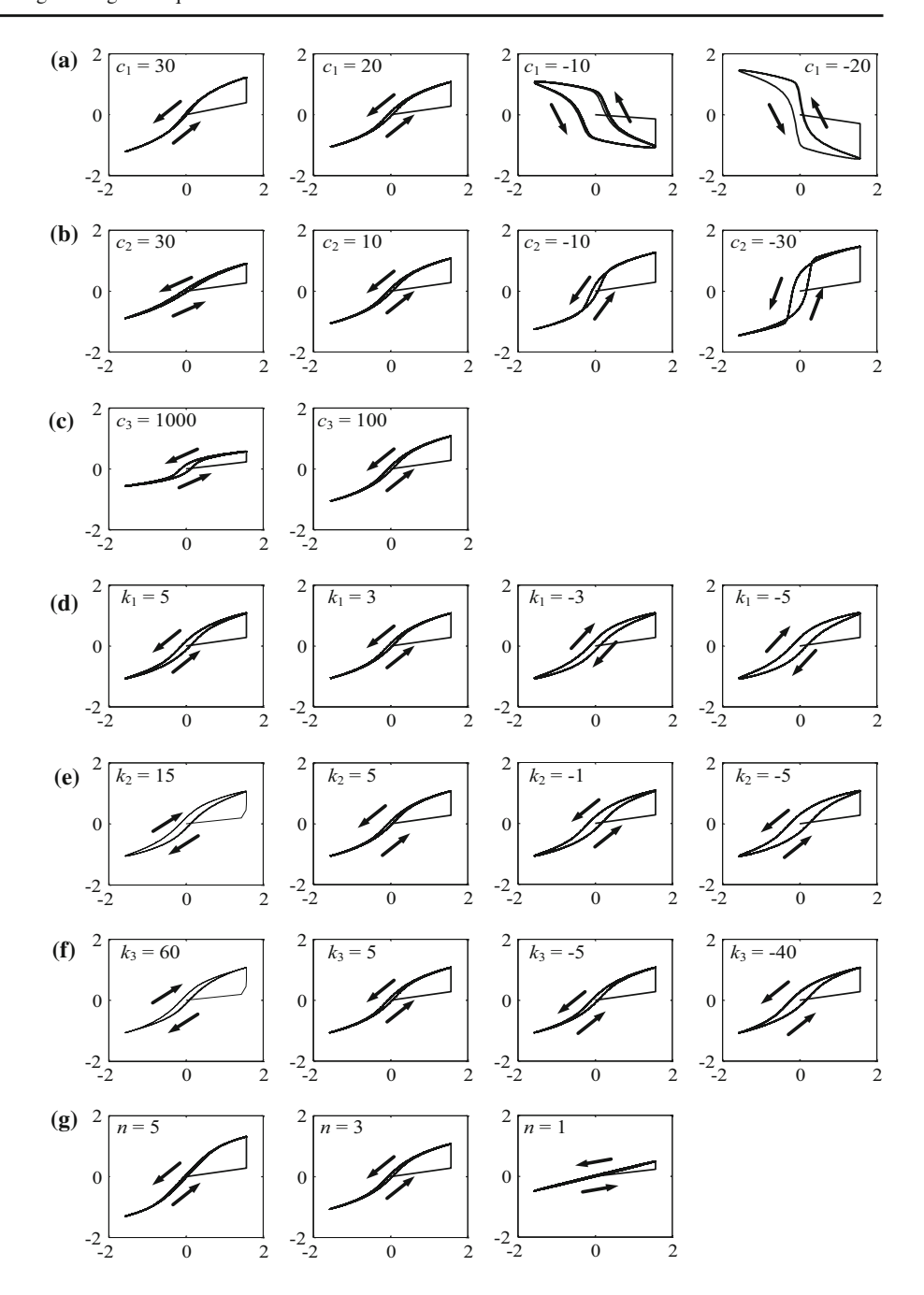
$$y = F_{\text{mr}} = \underbrace{\begin{bmatrix} 0 & A_f \end{bmatrix}}_{\mathbf{C}} \underbrace{\begin{bmatrix} x_1 \\ x_2 \end{bmatrix}}_{\mathbf{x}} \quad (14)$$

Accordingly, **B** and **d** correspond to the input matrix and input vector of the damper, respectively, and the damper force, $F_{\rm mr}$, is the hysteresis output, which is measurable from the piston load cell. Again, $F_{\rm mr}$ is linked to x_2 by multiplying A_f , and A_f is equal to the maximum amplitude of $F_{\rm mr}$.

According to the expressions in Eq. (12)–(14), velocity-force diagrams with a series of different parameters are shown in Fig. 6 to illustrate the fitting strategies. The given parameters are summarized in Table 1, and the simulation work was conducted in the Simulink environment, where the sinusoidal excitation had a frequency of 0.25 Hz and a unitary amplitude. The principal pattern of the hysteresis curve with respect to the path direction, area, shape, slope, and force magnitude can be observed in Fig. 6. First, the shape, slope, path, and area of the hysteresis loops are discussed. Figure 6 shows that c_1 and c_2 control the shape and area of the post- and pre-yield sections. As c2 increased, $F_{\rm mr}$ behaved more linearly, and the post- and preyield sections became obscure. In addition, as c_1 and nincreased, the slope of the curve for the pre-yield section became steep, and an increase in c_3 reduced the slop of the curve for the post-yield section. Regarding effective stiffness, variations in k_1, k_2 , and k_3 caused the hysteresis loops to be clockwise or counterclockwise. In addition, these variations controlled the angle and area between the back-and-forth paths. Furthermore, the $F_{\rm mr}$ amplitude could be adjusted by increasing or reducing c_1 , c_2 , c_3 , and n, whereas changes in k_1 , k_2 , and k_3 had no notable influence on the $F_{\rm mr}$ amplitude. As a rule of thumb, a preliminary tuning method is suggested as follows. First, n and A_f are determined



Fig. 6 Fitting pattern with a series of parameters given in Table 1. The sinusoidal excitation had a frequency of 0.25 Hz and a unitary amplitude. The *vertical* and *horizontal axes* denote the force and velocity signals, respectively



in a relatively straightforward manner according to the slope of the curve for the post-yield section and the $F_{\rm mr}$ peak. Second, c_1 , c_2 , and c_3 with respect to the hysteresis loop slope and area are defined in an iterative trial-and-error procedure. Third, k_1 , k_2 , and k_3 are used to refine the horizontal width changes without affecting the maximum amplitude of $F_{\rm mr}$. The tuning

procedure is summarized in Fig. 4b and is consistent with that shown in Fig. 4a.

Identification results for a 3-kN MR damper studied at the National Center for Research on Earthquake Engineering, Taiwan, are presented. The MR damper was subjected to a series of voltage signals from 0 to 0.8 V under 2 Hz sinusoidal excitations; the data sam-



Table 1 Applied parameters for Fig. 6 with $A_f = 2$

	c_1	c_2	c_3	k_1	k_2	k_3	n
(a)	-20, -10, 20, 30	10	100	3	5	5	3
(b)	20	-30, -10, 10, 30	100	3	5	5	3
(c)	20	10	100, 1000	3	5	5	3
(d)	20	10	100	-5, -3, 3, 5	5	5	3
(e)	20	10	100	3	-5, -1, 5, 15	5	3
(f)	20	10	100	3	5	-40, -5, 5, 60	3
(g)	20	10	100	3	5	5	1, 3, 5

Fig. 7 Identification results for a 3-kN MR damper under 2 Hz sinusoidal excitations. The fitted parameters are summarized in Table 2. The *left-hand column* shows displacement—force plots, and the *right-hand column* shows velocity—force plots. The *gray dotted lines* are the experimental results, and the *black solid lines* are the simulation results

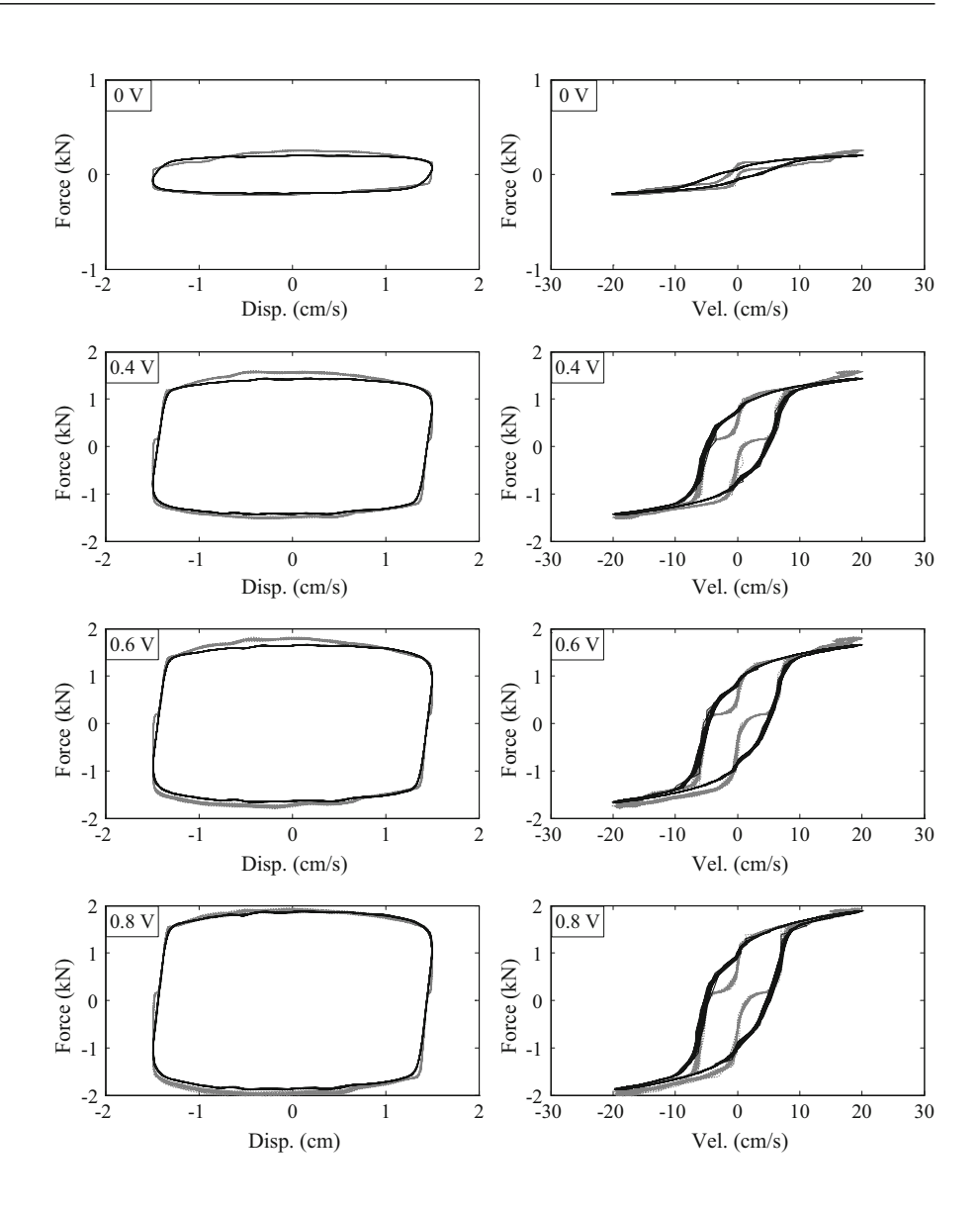




Table 2 Parameter identification results of a 3-kN MR damper under 2 Hz sinusoidal excitations

Voltage (V)	c_1	c_2	<i>c</i> ₃	k_1	k_2	k_3	n	A_f
0	10	100	350	50	800	0	5	0.25
0.2	10	10	330	40	650	0	5	1
0.3	10	10	320	36	520	0	5	1.4
0.4	10	10	320	34	480	0	5	1.6
0.5	10	10	280	33	470	0	5	1.7
0.6	10	10	280	32	450	0	5	1.8
0.8	10	10	250	30	400	0	5	2

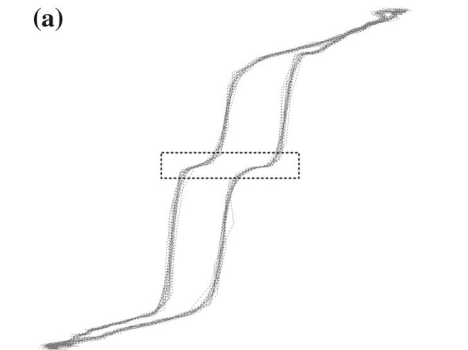
pling time was 0.005 s, and the experiment was based on the dSPACE real-time hardware. In Fig. 7, the measured $F_{\rm mr}$, d, and d data are drawn using gray dotted lines, and the simulated responses based on Eq. (12) are plotted using black solid lines. For brevity, only the cases of 0, 0.4, 0.6, and 0.8 V are shown, and the identified parameters for all cases are summarized in Table 2. As shown in Fig. 7, the measured and simulated input-output curves generally show a high level of agreement. However, the right-hand column of Fig. 7 exhibits an obvious mismatch, while the $F_{\rm mr}$ and dsignals approached zero. The modeling errors resulted from deadzone dynamics due to joint backlash, because repeated testing of the MR damper caused mechanical wear. A deadzone occurred when the actuator piston moved, but the damper force was not generated. When the deadzone dynamics were artificially removed, as shown in Fig. 8, the hysteresis loop pattern became similar to that shown in Fig. 1b. However, this identifi-

cation still preserved the deadzone dynamics to keep the results realistic. In future studies, the unwanted deadzone can be reduced by improving the experimental setup. Furthermore, to evaluate the robustness of the predicted models, the experimental data with 1 Hz sinusoidal and random excitations were compared for the cases of 0, 0.4, 0.6, and 0.8 V cases in Fig. 9, and the coefficients were fixed according to Eq. (12) and Table 2. Although noticeable fitting errors occurred, the models still captured a reasonable pattern and route for the hysteresis curves.

4 Conclusion

This paper proposes a new Duffing-like equation for modeling hysteresis dynamics. This Duffing-like model uses a second-order, continuous nonlinear ordinary differential equation to predict the hysteresis curve. When the input excitation and hysteresis output, i.e., d and y, are defined, the dynamics-based Duffinglike equation can model and analyze the input-output behavior in a systematic and traceable manner. The proposed model can facilitate numerical computation, stability analysis, and control design processes for the semi-active control of the MR dampers. In addition, the study can be extended and used to identify other mechanical, material, and structural systems that have hysteresis dynamics. In future research, attention will be given to more in-depth studies of (a) a systematic and optimal approach for parameterizing and refining the coefficients of the model; (b) a unified, frequencydependent model for circumventing time-varying input

Fig. 8 Velocity–force testing results for the 0.4V case: a the deadzone dynamics in the *dotted-line box* were measured; b because the deadzone was removed, the *curves* show proper hysteresis dynamics



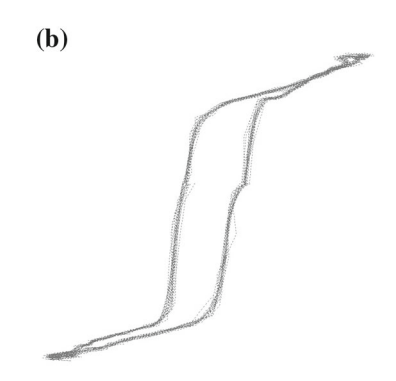
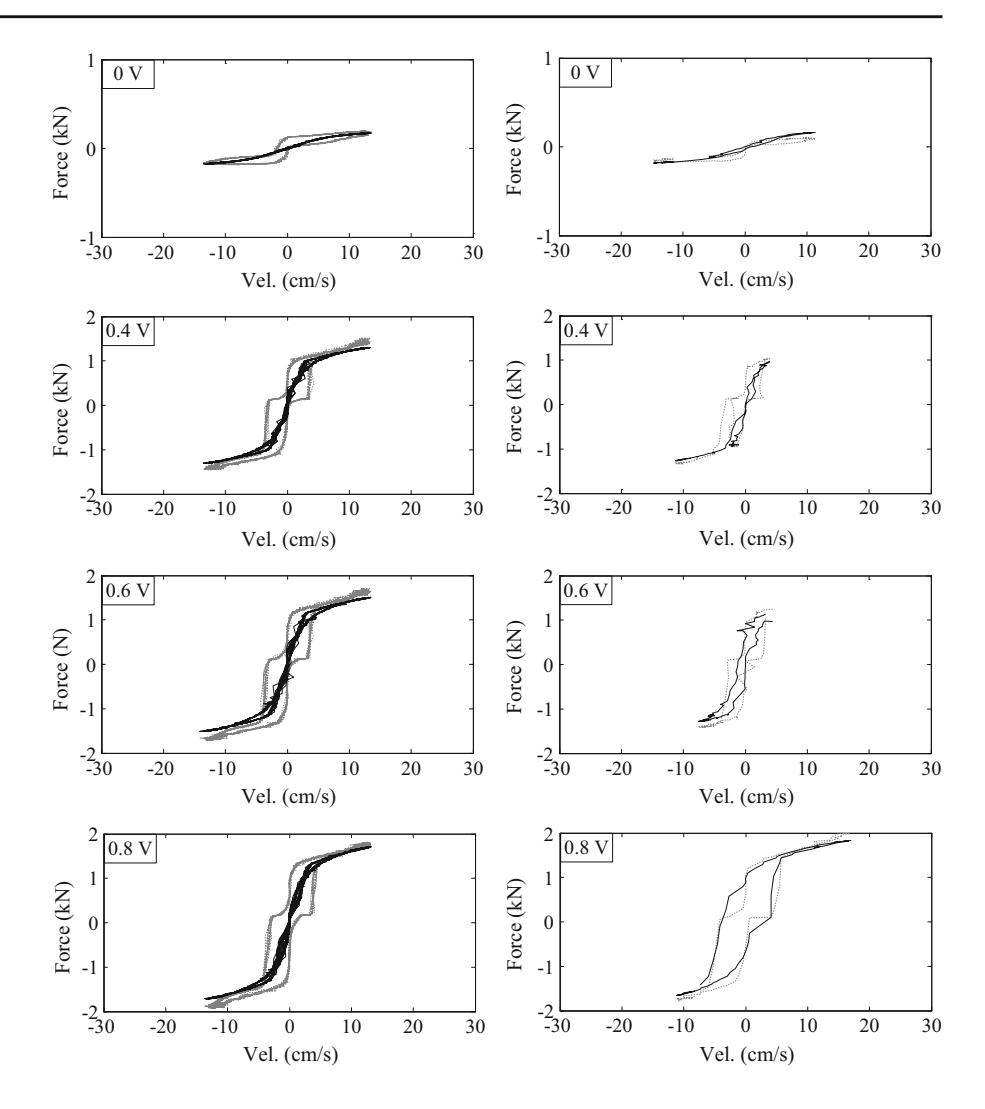




Fig. 9 Using the identified MR damper models in Table 2 to fit the experimental data under 1 Hz sinusoidal and random excitations. Only the velocity–force plots are shown. The *gray lines* represent the experimental results, and the *black lines* represent the simulation results



excitations; and (c) a semi-active control design for MR damper force.

Acknowledgments The authors gratefully acknowledge the support of the Taiwan Ministry of Science and Technology, under grant 102-2625-M-007-001- 'Development and Application of Model-Reference Semi-Active Control Methods for Magnetorheological Damper', and National Center for Research on Earthquake Engineering, for the support in the pursuance of this work.

References

 Spencer, B.F., Jr., Dyke, S.J., Sain, M.K., Carlson, J.D.: Phenomenological model for magnetorheological dampers. J. Eng. Mech. 123(3), 230–238 (1997). doi:10.1061/ (asce)0733-9399(1997)123:3(230)

- Wang, D.H., Liao, W.H.: Magnetorheological fluid dampers: a review of parametric modelling. Smart Mater. Struct. 20(2), 023001 (2011)
- Dimock, G.A., Lindler, J.E., Wereley, N.M.: Bingham biplastic analysis of shear thinning and thickening in magnetorheological dampers. Proceedings of SPIE 3985, Smart Structures and Materials 2000: Smart Structures and Integrated Systems, 444. (2000)
- Wereley, N.M., Pang, L., Kamath, G.M.: Idealized hysteresis modeling of electrorheological and magnetorheological dampers. J. Intell. Mater. Syst. Struct. 9(8), 642–649 (1998). doi:10.1177/1045389x9800900810
- Nakashima, M.: Development, potential, and limitations of real-time online (pseudo-dynamic) testing. Philos. Trans. R. Soc. Lond. Ser. A Math. Phys. Eng. Sci. 359(1786), 1851– 1867 (2001). doi:10.1098/rsta.2001.0876
- Dyke, S.J., Spencer, B.F., Sain, M.K., Carlson, J.D.: Modeling and control of magnetorheological dampers for seismic response reduction. Smart Mater. Struct. 5(5), 565–575 (1996). doi:10.1088/0964-1726/5/5/006



- Ikhouane, F., Rodellar, J.: Systems with Hysteresis Analysis, Identification and Control Using the Bouc-Wen Model. John Wiley and Sons, Chichester (2007)
- 8. Caterino, N., Spizzuoco, M., Occhiuzzi, A.: Understanding and modelling the physical behaviour of magnetorheological dampers for seismic structural control. Smart Mater. Struct. **20**(6), 065013 (2011)
- Yang, G., Spencer, B., Jung, H., Carlson, J.: Dynamic modeling of large-scale magnetorheological damper systems for civil engineering applications. J. Eng. Mech. 130(9), 1107–1114 (2004). doi:10.1061/(ASCE)0733-9399(2004)130: 9(1107)
- Tusset, A., Balthazar, J.: On the chaotic suppression of both ideal and non-ideal duffing based vibrating systems, using a magnetorheological damper. Differ. Equ. Dyn. Syst. 21(1– 2), 105–121 (2013). doi:10.1007/s12591-012-0128-4
- Ikhouane, F., Rodellar, J.: On the hysteretic Bouc-Wen model. Nonlinear Dyn. 42(1), 63–78 (2005). doi:10.1007/ s11071-005-0069-3
- Cetin, S., Zergeroglu, E., Sivrioglu, S., Yuksek, I.: A new semiactive nonlinear adaptive controller for structures using MR damper: Design and experimental validation. Nonlinear Dyn. 66(4), 731–743 (2011). doi:10.1007/ s11071-011-9946-0
- Sims, N.D., Holmes, N.J., Stanway, R.: A unified modelling and model updating procedure for electrorheological and magnetorheological vibration dampers. Smart Mater. Struct. 13(1), 100 (2004)
- Jiang, Z., Christenson, R.E.: A fully dynamic magnetorheological fluid damper model. Smart Mater. Struct. 21(6), 065002 (2012)

- Visintin, A.: Differential Models of Hysteresis. Springer, Berlin (1994)
- Duffing, G.: Erzwungene Schwingungen bei veränderlicher Eigenfrequenz und ihre Technische Bedeutung. R, Vieweg & Sohn, (1918)
- Korsch, H.J., Jodl, H.-J., Hartmann, T.: Chaos: A Program Collection for the PC. Springer, Berlin (2008)
- Hu, H., Dowell, E., Virgin, L.: Resonances of a harmonically forced Duffing oscillator with time delay state feedback. Nonlinear Dyn. 15(4), 311–327 (1998). doi:10.1023/ A:1008278526811
- Kovacic, I., Rand, R.: About a class of nonlinear oscillators with amplitude-independent frequency. Nonlinear Dyn. 74(1–2), 455–465 (2013). doi:10.1007/s11071-013-0982-9
- Moon, F.C., Holmes, P.J.: A magnetoelastic strange attractor. J. Sound Vib. 65(2), 275–296 (1979). doi:10.1016/0022-460X(79)90520-0
- Pandey, M., Rand, R., Zehnder, A.: Frequency locking in a forced Mathieu-van der Pol-Duffing system. Nonlinear Dyn. 54(1–2), 3–12 (2008). doi:10.1007/s11071-007-9238-x
- Slotine, J.-J.E., Li, W.: Applied Nonlinear Control. Pearson Education, Taiwan (2005)
- Tu, J.-Y., Chen, T.-C., Lin, P.-Y.: Using Duffing equation to model magnetorheological damper dynamics. In: The 6th world conference on structural control and monitoring, Barcelona, Spain, 15–17 July (2014)

